

Adaptive Optics Spectroscopy: Preliminary Theoretical Results

Jian Ge^a, Roger Angel^a, David Sandler^{a,b}, Chris Shelton^a, Don McCarthy^a, Jim Burge^a

^aSteward Observatory, The University of Arizona,
Tucson, AZ 85721 USA

^bThermoTrex Corporation, 10455 Pacific Center Court
San Diego, CA 92121 USA

ABSTRACT

Diffraction-limited spectroscopy with adaptive optics (AO) has several advantages over traditional seeing-limited spectroscopy. First, high resolution can be achieved without a large loss of light at the entrance slit of the spectrograph. Second, the small AO image width allows the cross-dispersed orders to be spaced closer together on the detector, allowing a large wavelength coverage. Third, AO spectrograph optics are slow and small, costing much less than for a traditional spectrograph. Fourth, small AO images provide high spatial resolution. Fifth, scattered light is less problematic. And last, the small entrance slit of the spectrograph can get rid of much of the sky background to obtain spectra of faint objects.

We have done theoretical calculations and simulations for infrared spectroscopy at the MMT 6.5 m with laser guide star AO, which provides almost full sky coverage. The results show we can expect 40-60% of the photons from a unresolved source within 0.2 arcsec diameter circle for J, H, K, L and M bands under typical atmospheric seeing condition at 2.2 micron ($r_0 = 1.0$ m, $t_0 = 21$ ms, $\theta_0 = 15$ arcsec and $d_0 = 25$ m). Therefore, the spectrograph entrance slit size should match the 0.2 arcsec image to obtain high throughput. Higher resolution can be achieved by narrowing down the slit size to match the diffraction-limited image core size of about 0.1 arcsec in the infrared. However, the throughput will be correspondingly reduced by a factor of two. Due to the limited atmospheric isoplanatic angle in the J, H and K bands, the encircled photon percentage within 0.2 arcsec diameter drops from 40-60% when the object is at the laser pointing direction to 20-40% when the object is about 30 arcsec away from the laser direction. Therefore, the useful field of view for AO multiple object spectroscopy is about 60 arcsec. Further studies of IR background (sky and thermal) and IR detector performance show that spectral resolution of $R = 2,000$ can take full advantage of AO images without much penalty due to the dark current of the IR detector and IR OH sky emission lines.

We have also studied natural guide star AO spectroscopy. Though sky coverage for this kind of spectroscopy at the MMT 6.5 m is very limited, a bright star provides much better performance than the laser guide star AO spectroscopy. About 40-70% photons are concentrated within 0.1 arcsec diameter for guide stars brighter than 13 magnitude. Therefore, higher resolution and high throughput can be obtained simultaneously, given a bright enough natural guide object. The field-of-view for multiobject spectroscopy using a natural guide star is similar to that for laser guiding.

Keywords: Adaptive Optics, Spectroscopy, Encircled Energy, Point Spread Function

1. INTRODUCTION

Adaptive optics (AO) promises revolutionary advances in imaging power for ground-based optical and infrared astronomical telescopes by eliminating the wave-front distortion caused by atmospheric turbulence. The AO corrected images will be nearly diffraction-limited, which is about a factor of ten times smaller than that limited by the atmospheric seeing for current 4 m class telescopes. For the largest of the new generation of telescopes, the most dramatic gain is possible, permitting an imaging performance of almost two orders of magnitude (100 times).

Though adaptive optics has a big impact on improving ground-based telescope image quality, it cannot provide ideal diffraction-limited images in principle, due to the limited photon flux available from the reference source, finite

Other author information: (Send correspondence to Jian Ge)

J. G.: Email: jge@as.arizona.edu; WWW: <http://qso.as.arizona.edu/~jge>; Telephone: 520-621-6535; Fax: 520-621-1532

response time and subaperture size of the AO systems (Sandler et al. 1994). The AO corrected images therefore consist of two components: a diffraction-limited core and a broad seeing-limited halo (Beckers 1993), which make the design of AO instruments different from that of seeing limited instruments.

The much sharpened AO images have two main applications in astronomy research; imaging and spectroscopy. The two are closely related but not the same. The main focus of direct high resolution imaging is to sharpen the diffraction limited image core, to maintain stable uniform point spread function (PSF) in both spatial and temporal domains. On the other hand, the most concern of the AO spectroscopy is the flux concentration. The different demands for these two different applications determine different instrument design parameters.

The application of adaptive optics in astronomy is still in its early phase and the design of AO optimized instruments, especially the spectrographs, is a new territory being opened for exploration. In seeing limited domain, the best resolution of a spectrograph is coupled to the telescope diameter, the larger the aperture size, the lower the spectral resolution for the normal available grating size. This coupling limited the best spectral resolution of traditional spectrographs to $R \sim 50,000$ for 4 m class telescopes (Vogt & Schroeder 1987). In order to obtain higher resolution, all kind of tricks such as image slicers, pupil slicers, grating mosaics etc have been applied and resulted in very large and expensive spectrographs at the Nasmyth or Coude focuses (e.g. Diego et al. 1995; Vogt et al. 1994; Tull et al. 1994). However, in the AO diffraction limited domain, because the AO corrected image size (i.e. diffraction limited core size) decreases proportionally with telescope aperture size, the coupling of spectrograph size with telescope aperture is removed. Very high resolution spectrographs can be made from normal size gratings. As the results, the next generation AO optimized high resolution spectrographs will have smaller overall scale, higher efficiency and also cost much less. As the first demonstration of next generation AO spectrographs, we have built a prototype AO cross-dispersed echelle spectrograph with a $125 \times 250 \text{ mm}^2$ R2 echelle grating at Steward Observatory and tested at Starfire Optical Range 1.5 m AO telescope. The spectrograph can provide spectral resolution up to $R = 700,000$ (Ge et al. 1996). Because of the much smaller image size, a large amount of cross dispersed orders can be packed and recorded on the detector, and thus a factor of 100 times larger wavelength coverage over similar resolution traditional spectrographs was achieved (e.g. Diego et al. 1995; Lambert et al. 1990; Ge et al. 1996). And because of the much smaller image size, AO spectrographs can record astronomical phenomena of much smaller scale structure (Bacon et al. 1995). Further, smaller entrance slit used in the AO spectrographs can help to block most sky background, especially in the IR where the sky background is about 100 times brighter than in the visible, so much fainter objects can be observed.

In this paper, we will first set out the types of error that arise in the adaptive optics systems and how they together affect overall performance of AO spectroscopy. Then we will use the MMT 6.5 m AO system under construction as an example to introduce the results from the semi-empirical analytical calculations and direct Monte Carlo simulations and relate these computational results to the design of AO spectrographs.

2. THEORETICAL CONSIDERATIONS

Adaptive optics residual error contributions can be divided into tilt and higher order error terms (Parenti 1992; Sandler et al. 1994). AO systems often apply corrections to these aberrations separately. The low order tilt errors are compensated by the tilt-control element and the high order errors are corrected by the deformable mirror. Therefore the overall image quality can be described as

$$S_{tot} = S_{tilt} S_{HO} \quad (1)$$

where S_{tot} is the total system Strehl ratio (SR), S_{tilt} is the SR for the tilt error correction only and S_{HO} is the SR for the high-order aberration correction only.

2.1. Tilt Errors

The tilt, caused by the effects of atmospheric jitter, has a longer correlation time due to its large scale. Three major sources contribute to the residual tilt errors: anisoplanatism (σ_{iso}), centroid uncertainty (σ_{cent}) and temporal decorrelation (σ_{temp}) (Sandler et al. 1994). The total one-axis mean square tilt error can be written as

$$\sigma_{tilt}^2 = \sigma_{iso}^2 + \sigma_{cent}^2 + \sigma_{temp}^2. \quad (2)$$

The tilt anisoplanatism is caused by the different atmospheric wedge traced by the light from the tilt sensing field star and from the science object. It can be described as the average of tilt errors in the longitudinal and the lateral directions,

$$\sigma_{iso}^2 = \frac{(\sigma_{iso}^x)^2 + (\sigma_{iso}^y)^2}{2}, \quad (3)$$

where the longitudinal tilt anisoplanatism,

$$(\sigma_{iso}^x)^2 = [0.0472\left(\frac{\theta}{\theta_0}\right)^2\left(\frac{D}{r_0}\right)^{-1/3} - 0.0107\left(\frac{\theta}{\theta_0}\right)^4\left(\frac{D}{r_0}\right)^{-7/3}]\left(\frac{\lambda}{D}\right)^2, \quad (4)$$

and the lateral tilt anisoplanatism,

$$(\sigma_{iso}^y)^2 = [0.0157\left(\frac{\theta}{\theta_0}\right)^2\left(\frac{D}{r_0}\right)^{-1/3} - 0.00214\left(\frac{\theta}{\theta_0}\right)^4\left(\frac{D}{r_0}\right)^{-7/3}]\left(\frac{\lambda}{D}\right)^2, \quad (5)$$

where r_0 is the atmospheric turbulence coherence length, and θ_0 is the size of the isoplanatic angle, D is the telescope aperture size and λ is the tilt sensing wavelength (see Sandler et al. 1994 for details).

The temporal tilt decorrelation is caused by the delay between measuring and compensating for the atmospheric wedge. The average mean-square temporal tilt error can be expressed as

$$\sigma_{temp}^2 = 0.031\left(\frac{T}{t_0}\right)^2\left(\frac{r_0}{D}\right)^{1/3}\left(\frac{\lambda}{D}\right)^2, \quad (6)$$

where t_0 is the atmospheric coherence time and T is the delay time between sensing and correcting.

Due to the limited photon flux available from the tilt field star and detector intrinsic noise, the exact centroid of the tilt guide star image cannot be precisely measured. The resulting error is called the tilt centroiding error, which can be written as

$$\sigma_{cent}^2 = \frac{\alpha^2 w^2}{N}\left(1 + \frac{4n^2}{N}\right)\left(\frac{\lambda}{D}\right)^2, \quad (7)$$

where the parameter α depends on D/r_0 , $\alpha = 0.76 - 1.11$ for $D/r_0 = 7-10$, N is the total detected photon number, n is the detector readout noise, w is the FWHM of the image in units of the diffraction-limited image width λ/D .

2.2. High Order Errors

The contributions to high order correction errors are fitting (σ_{fit}), reconstruction (σ_{rec}), temporal-decorrelation (σ_{time}), high-order anisoplanatism (σ_{hoiso}) and focus anisoplanatism (σ_{cone}) if laser guide star is used. The total mean-square high-order correction error is

$$\sigma_{HO}^2 = \sigma_{fit}^2 + \sigma_{hoiso}^2 + \sigma_{rec}^2 + \sigma_{time}^2 + \sigma_{cone}^2. \quad (8)$$

Because of its finite number of actuators, the spatial frequency components with scales smaller than a subaperture size cannot be corrected by the adaptive deformable mirror. The resulting wave-front error is called fitting error, which is further written as

$$\sigma_{fit}^2 = c\left(\frac{d}{r_0}\right)^{5/3}, \quad (9)$$

where $c \approx 0.29$, depends on the actuator arrangement and d is the subaperture size (Greenwood & Parenti, 1994; Ellerbroek, 1991; Rigaut 1994).

High-order anisoplanatism arises from the angular separation θ between the reference source being sensed and corrected and the object being imaged. A good approximation for this high order anisoplanatism is

$$\sigma_{hoiso}^2 = \sigma_{\phi}^2 - \ln[1 + 0.9736E + 0.5133E^2 + 0.2009E^3 + 0.0697E^4 + 0.02744E^5], \quad (10)$$

where

$$E = 6.88\frac{\mu_2}{\mu_0}\left(\frac{\theta}{D}\right)^2\left(\frac{D}{r_0}\right)^{5/3}, \quad \sigma_{\phi}^2 = \left(\frac{\theta}{\theta_0}\right)^{5/3}, \quad \mu_n = \sec^{n+1}(\zeta) \int_0^{\infty} h^n C_n^2(h) dh, \quad (11)$$

$C_n^2(h)$ is the index-of-refraction structure constant at altitude h , ζ is the zenith angle (Greenwood & Parenti 1994; Sasiela 1993). This approximation gives accurate Strehl ratio values down to values of 0.2.

The high order temporal decorrelation error is caused by the change of the atmospheric wedges over each subaperture over the wavefront sensor delay time, Δt . The error is approximately

$$\sigma_{time}^2 = \left(\frac{\Delta t}{t_0}\right)^{5/3}. \quad (12)$$

The reconstruction error has the same general form as the centroiding error for tilt correction because the errors introduced by centroiding uncertainty due to the photon noise and detector noise over each subaperture result in a rms wavefront error in the final reconstructed wave front. It can be written as

$$\sigma_{rec}^2 = \frac{4\pi^2 G \alpha^2 w^2}{N} \left(1 + \frac{4n^2}{N}\right) \left(\frac{\lambda_0}{\lambda}\right)^2, \quad (13)$$

where $G \approx 0.5$, which depends on the geometry of the reconstructor, λ_0 is the sensing wavelength and λ is the science wavelength.

Focus anisoplanatism is the effect where light from a laser beacon (finite height) does not sample the same turbulence as the light from the observed target does (infinite height). The cone error is expressed as

$$\sigma_{cone}^2 = \left(\frac{D}{d_0}\right)^{5/3}, \quad (14)$$

where d_0 is a length-like quantity defined by Fried (1994).

2.3. The AO Corrected Images for Spectroscopy

Because of the existence of the low (σ_{tilt}) and high order residual errors (σ_{HO}) after the AO correction, the AO corrected images are not perfectly diffraction limited. They generally consist of two components, a diffraction limited core and a broad uncorrected “seeing” halo. The diffraction limited core appears after the low spatial frequency wavefront errors (such as tilt error) are reduced. The halo components decrease once the higher spatial frequency errors are reduced. Most previous astronomical AO systems are low order systems. Though they can provide diffraction-limited image core for high resolution imaging, the energy concentration within small angular diameter is relatively low, therefore these systems are not ideal for AO spectroscopy. However, the existing high order AO systems at the SOR 1.5 m telescope and Mt. Wilson 2.5 m telescope have the power to concentrate about 50% photons within central $0.2''$. They are certainly suitable for AO spectroscopy (Ge et al. 1996). Moreover, some new AO systems being designed and built at large telescopes such as the MMT 6.5 m will provide high order compensation which can largely improve the photon flux concentration ability in the IR for high throughput AO spectroscopy.

3. THEORETICAL STUDY RESULTS

A number of useful methods have been applied to study the AO performance including direct Monte Carlo computer simulation of the whole AO system (Sandler et al. 1994), semi-empirical analysis (Parenti 1992; Ridgway 1994) and the evaluations in terms of residual mean-square phase distortion and the associated optical transfer function (OTF) (Ellerbroek 1994; Ellerbroek et al. 1994). In this paper, we will apply the first two methods to analyze the performance of the AO system under construction for the MMT 6.5 m, and to relate them to the AO spectrograph design.

3.1. Semi-empirical Calculations

Previous study by Parenti (1992) demonstrates that in a long-exposure image corrected by an AO system the randomly fluctuating sidelobes appearing in a short-exposure image smooth out to form a broad quasi-Gaussian shape background skirt, which is determined by uncorrected beam motion. The diffraction-limited primary lobe shown in the short integration forms another sharp quasi-Gaussian profile overlapped on the broad background profile. The PSF of the resulting image in a long exposure time is the sum of these two quasi-Gaussian functions.

Therefore, important parameters to describe the AO performance such as Strehl ratio, encircled energy and resolution can be expressed by analytical formulae which make the system performance study much easier than through other methods. For the most intermediate cases, the results from this simple method agree reasonably well with much complicated computer-simulation results as shown in the next subsection and agree with the real time observation results as well. However, for the very poor and very good correction cases, the results from this method represent the expected asymptotic behavior.

In this approach, the width of the AO corrected diffraction limited core is expressed as

$$W_c = \sqrt{(1.22\frac{\lambda}{D})^2 + (2.7\sigma_{tilt})^2}, \quad (15)$$

and the width of the uncorrected halo can be written as

$$W_h = 1.22\frac{\lambda}{r_0}. \quad (16)$$

The central intensity of the core component is

$$I_c = \frac{\exp(-\sigma_{HO}^2)}{1 + 4.94(\frac{D}{\lambda})^2\sigma_{tilt}^2}, \quad (17)$$

and the peak intensity of the halo component is

$$I_h = \frac{1 - \exp(-\sigma_{HO}^2)}{1 + (\frac{D}{r_0})^2}. \quad (18)$$

Therefore, the PSF can be approximately expressed by (Ridgway 1994)

$$I(\alpha) = I_c \exp(-\frac{4\ln 2}{W_c^2}\alpha^2) + I_h \exp(-\frac{4\ln 2}{W_h^2}\alpha^2), \quad (19)$$

where we have assumed Gaussian shapes for both components, α is the angle from the image center. With this definitions, the Strehl ratio is the value in Eq. 19 when $\alpha = 0$, i.e.

$$SR = I(0) = I_c + I_h. \quad (20)$$

The encircled energy within β angle is the integral of $I(\alpha)$, or

$$E(\beta) = \int_0^\beta I(\alpha) 2\pi\alpha d\alpha = \frac{1}{W_c^2 I_c + W_h^2 I_h} [W_c^2 I_c (1 - \exp(-\frac{4\ln 2\beta^2}{W_c^2})) + W_h^2 I_h (1 - \exp(-\frac{4\ln 2\beta^2}{W_h^2}))]. \quad (21)$$

As an example, Table 1 shows direct comparisons between the theoretical predictions from the semi-empirical analysis and observation results from the Mt. Wilson 2.5 m telescope AO system. The atmospheric parameters at 2.2 μm , $r_0 = 1.8$ m or 0.4'' seeing, wind velocity 21 m s⁻¹ or $t_0 = 15$ ms were applied in order to match the theoretical predictions with the observation values in the R band. Subaperture size of 0.156 m, wavefront sensor delay time of 5.0 ms and tilt correcting delay time of 5.0 ms were also used in the calculations. The observed star is SAO 140094 with V = 6.6 mag. The resulting predicts from the first order theoretical analysis also reasonably match with the observation values in the other wavelength regions such as I, V and B bands.

In the following, we applied the semi-empirical formulae to explore the on-axis and off-axis performance of the MMT 6.5 m LGS and NGS AO systems. In the calculations, the laser beacon was assumed to point in the direction of the science object for high order correction and a H = 18 mag. field star 30'' away from the science object was used for the global tilt correction. The LGS therefore can provide image corrections for almost anywhere on the sky (Sandler et al. 1994). We further assumed that the wavefront sensor sensing and compensating time is 2 ms and global tilt time delay is 15 ms. The average values of the atmospheric parameters, $r_0 = 1.0$ m, $t_0 = 21.2$ ms, $d_0 = 25$ m and $\theta_0 = 15.4''$ at 2.2 μm were adopted. The laser is a 4 watts sodium laser, which is applied to the mesosphere

Table 1. Comparison between Theoretical and Observational Results for the Mt. Wilson 2.5 m Telescope NGS AO System.

Wavelength	SR(the)	SR(ob)	0.1''EE(the)	0.1''EE(ob)	0.2''EE(the)	0.2''EE(ob)
I(0.9 μ m)	0.34	0.36	22%	22%	46%	42%
R(0.7 μ m)	0.18	0.17	17%	17%	33%	35%
V(0.55 μ m)	0.07	0.09	10%	17%	23%	31%
B(0.44 μ m)	0.02	0.03	6%	8%	18%	22%

sodium layer to form a $R = 9.5$ mag. artificial sodium star. This is certainly achievable with the cw dye laser we are using at the MMT. For instance, recent simultaneous measurements of the sodium laser guide star return and mesospheric sodium column density at the MMT and CFA 60 inch telescopes on Mt. Hopkins show that a $R = 10$ mag. laser guide star formed from 1 watt projected sodium laser power on the sky when the sodium column density is about the annual mean value of $3.6 \times 10^9 \text{ cm}^{-2}$ (Ge et al. 1997). Table 2 shows the calculation results about the LGS AO system from the above empirical formulae.

Table 2. The Calculation Results for the MMT 6.5 LGS AO System Performance under the Typical Seeing Condition on Mt. Hopkins.

Bands	Strehl Ratio	50% Encircled Energy	80% Encircled Energy
J(1.25 μ m)	0.29	0.32''	0.75''
H(1.65 μ m)	0.40	0.12''	0.59''
K(2.2 μ m)	0.48	0.12''	0.36''
L(3.6 μ m)	0.56	0.16''	0.26''
M(4.8 μ m)	0.58	0.20''	0.32''

Figure 1 shows the results of LGS AO corrected image angular diameter versus wavelength in the near IR (1 - 5 μ m). The photon flux concentration strongly depends on wavelength. At the J band, uncorrected high order wavefront errors especially the focus anisoplanatism caused by the single laser beacon are significant, uncorrected "seeing" halo dominates the whole image, only about 30-40% photons are concentrated within 0.2'' central image area. In the H and K, the AO corrected diffraction-limited component begin to be dominant, 50-60% photons are within the same 0.2'' angular diameter. As the wavelength moves to the L and M bands, the AO corrected images are close to the diffraction-limit. However, the diffraction-limited core size is also getting larger at these longer wavelengths. Therefore there are about 40-50% photons concentrated within 0.2'' aperture.

Figure 2 shows the off-axis performance from the LGS AO system, which illustrates the relatively narrow corrected field-of-view. However, the corrected FOV strongly depends on the science wavelength. The useful FOV for J, H and K bands is generally less than $60'' \times 60''$, though the corrected FOVs in the L and M bands are expected to be larger.

Though the LGS AO system dramatically increases the sky coverage for science observations, a relatively wide slit size of 0.2'' is required to maintain high throughput for the IR spectroscopy. In order to obtain high spectral resolution such as $R \sim 100,000$, the IR spectrograph system turns out to be very large, which begin to push limits on designs of the IR cryogenic and mechanical systems. On the other hand, the NGS AO system is expected to perform much better in the short IR wavelength than the LGS AO because there is no focus anisoplanatism contribution to the residual high order wavefront aberrations. Figure 3 shows the calculation results of the MMT NGS AO performance under the average seeing conditions. As expected, the fractional energy concentration is much higher than that from the LGS AO system. For instance, the fractional encircled energy is about 20-40% within 0.1'' angular diameter for a NGS with $V \sim 14$ magnitude, and 40-70% for a NGS guide star brighter than 13 magnitude. Therefore, in the very limited observation case when there is a bright NGS in the field, especially when the science object is the NGS itself,

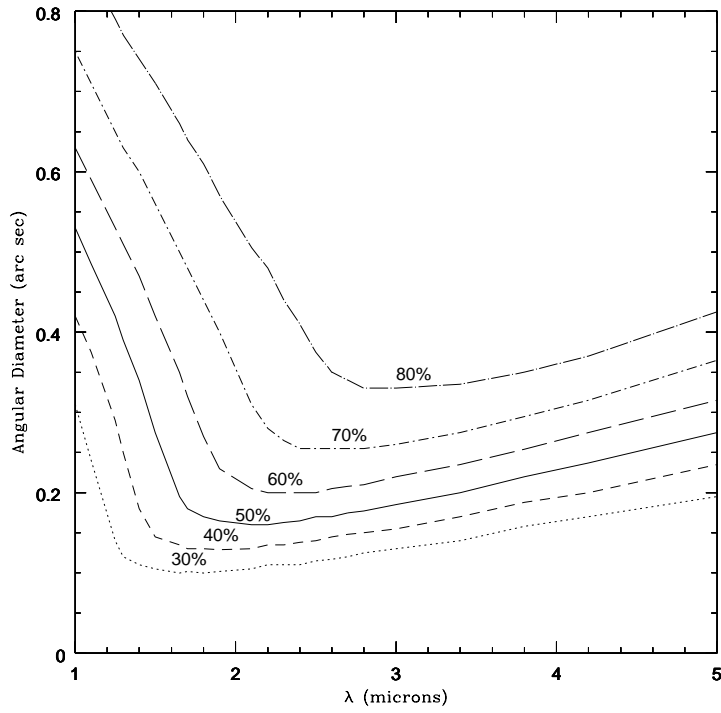


Figure 1. The image angular diameter vs wavelength at the near IR for the MMT LGS AO system under the average seeing conditions. Different fractional encircled energy lines are drawn and marked.

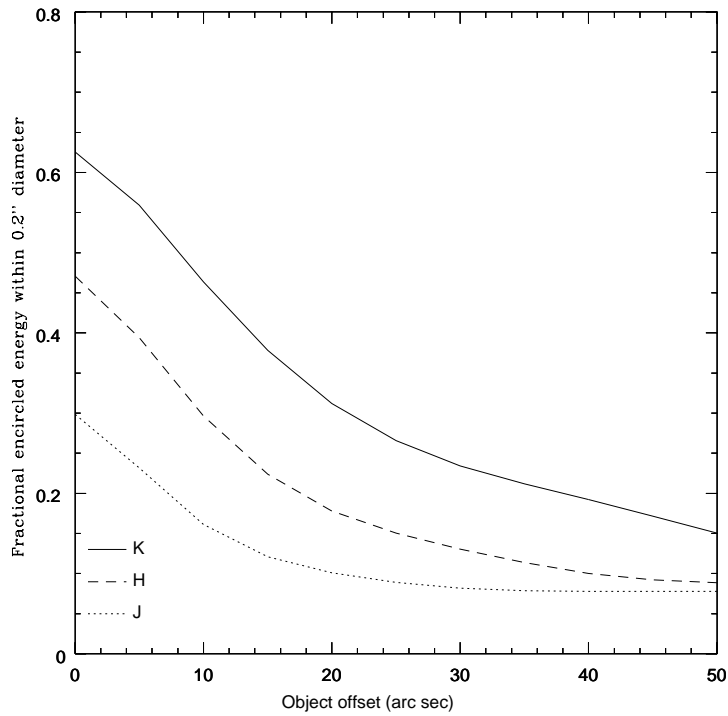


Figure 2. Fractional encircled energy within 0.2'' diameter at the J, H and K bands vs the angle between the laser beacon and science object for the MMT LGS AO system under the average seeing condition.

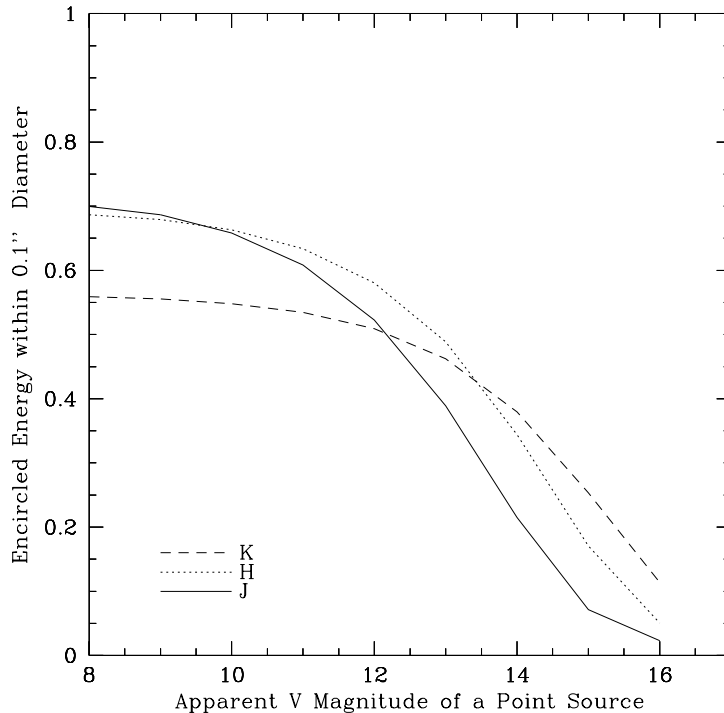


Figure 3. Fractional encircled energy vs apparent V magnitude of a point source with the MMT 6.5 m NGS AO system under the average seeing condition.

IR spectroscopy can be pursued with a $\sim 0.1''$ entrance slit, a factor of two higher spectral resolution can therefore be achieved.

3.2. Monte Carlo Simulations

This method has been used to study the LGS AO performance on 8-m telescopes (Sandler et al. 1994). The basic procedure is to generate a perfect plane wavefront and then let it pass through 10 to 20 Kolmogorov phase screens spaced between 3 to 20 km. The global tilt in the simulated distorted wavefront from a $H = 18$ mag. field star was sensed in the wavelength of $1.25\text{-}2.2 \mu\text{m}$ and the measured wavefront slopes across the 6.5 m aperture were used to remove the wavefront tilt from the science object, which is $30''$ away. Then the high order aberrations sensed by a simulated back-scattered laser beacon from the sodium layer (90 km altitude) in the direction of the science object were measured and applied to provide high order correction for the wavefront of the science object. The deformable mirror used for the high order correction has 13×13 actuators with the subaperture size of 0.5 m. Other parameters used in this simulation approach are the same as used in the above semi-empirical analysis. The output PSFs were used to measure the resulting Strehl ratio, fractional encircled energy, resolution etc.

In the simulations, we used the MK atmospheric model described in the paper by Sandler et al. (1994), corresponding to the atmospheric parameters of $r_0 = 1.0$ m, $t_0 = 21$ ms, $d_0 = 25$ m and $\theta_0 = 15.4''$ at $2.2 \mu\text{m}$, typical values on Mt. Hopkins. Figure 4 shows example image profiles in the K band for the diffraction-limited and the LGS AO corrected cases from the simulations. The Strehl ratio for the AO corrected image is 0.55. Compared to the ideal diffraction-limited image profile, the AO sharpened image shows that more photons spread out in the wing of the image profile. The whole profile indeed consists of a sharp Gaussian profile with the FWHM similar to the diffraction-limited core width and a much broader Gaussian profile (Parenti 1992). The broad seeing-like halo profile is caused by the residual high spatial frequency aberrations mainly contributed by the LGS focus anisoplanatism.

Figure 5 shows the fractional encircled energy versus angular diameter from the simulations. MMT 6.5 m LGS AO system can concentrate about 50% photon within $0.2''$ diameter for wavelength longer than $1.4 \mu\text{m}$. Once the correction goes to the shorter wavelength, the laser cone effect and fitting error become significant, and less photons

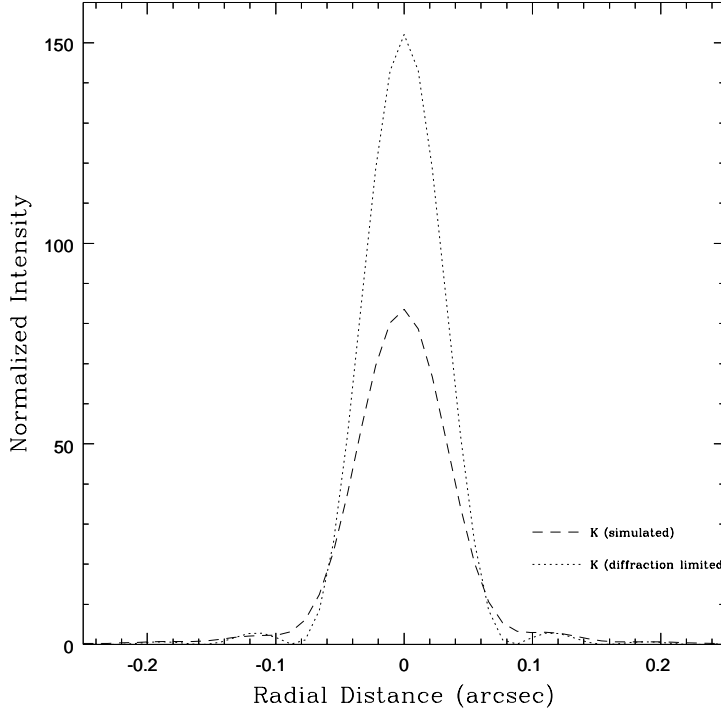


Figure 4. Simulated K band diffraction-limited and laser guide star AO corrected stellar image profiles from the MMT 6.5 m.

are within the diffraction limited core. Figure 5 further illustrates that the rest $\sim 30\%$ uncorrected photons from the MMT 6.5 m single beacon LGS AO system are widely distributed over a large area. This new result has important meaning for the IR spectrograph design.

Table 3 summarizes the simulation results in the J, H, K, L and M bands. Compared to the semi-empirical calculation results shown in the Table 2, the simulations show similar results on the 50% encircled energy in the whole near IR wavelengths, but gives lower Strehl ratios for the J and H bands, and higher SRs for the K, L and M bands, and also predicts different aperture sizes for the 80% encircled energy.

Table 3. The simulation results for the MMT 6.5 m LGS AO system performance under typical seeing condition on Mt. Hopkins.

Bands	Strehl Ratio	50% Encircled Energy	80% Encircled Energy
J	0.16	0.28''	0.80''
H	0.36	0.19''	0.73''
K	0.55	0.13''	0.65''
L	0.79	0.15''	0.50''
M	0.88	0.18''	0.50''
J(no AO)	0.02	0.45''	0.90''

4. DESIGN OF AO SPECTROGRAPHS

The preliminary results from the computer simulations and theoretical calculations demonstrate that astronomical adaptive optics with laser or natural guide stars cannot achieve ideal diffraction-limited images even at the longer IR wavelength region such as L and M bands. The shapes of the resulting AO corrected image profiles depend on

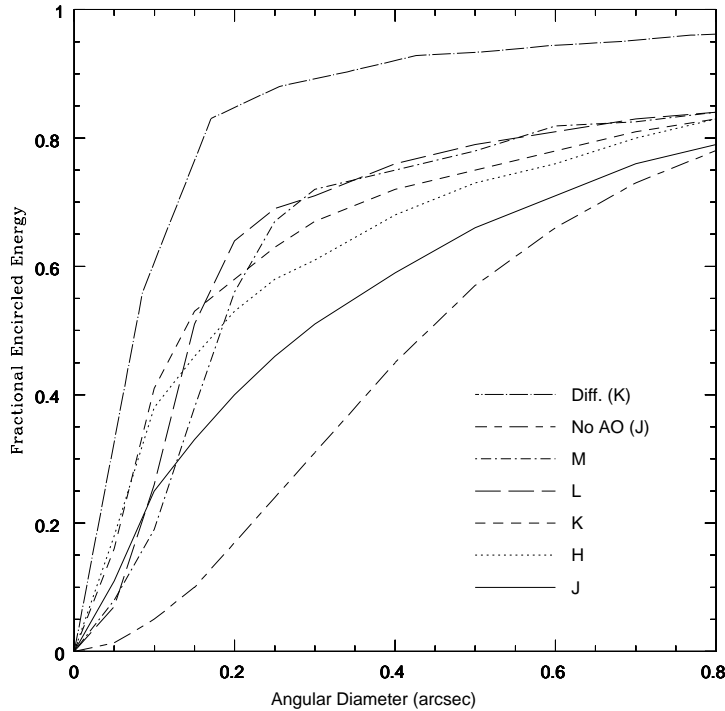


Figure 5. Fractional encircled energy vs angular diameter for the MMT LGS AO system under average seeing condition.

how well the low order and high order wavefront aberrations have been corrected, which can be easily affected by the instantaneous atmospheric conditions, guide star magnitudes and nature (LGS or NGS), and also AO correcting parameters. All these make the design of AO instruments, especially spectrographs, in some respects more complicated than for the seeing limit.

As shown above, in order to provide full sky coverage of the AO observations, laser guide star is required. The extra high order aberration from the LGS, focus anisoplanatism, is the dominant one in the whole IR wavelength range and will make a large fraction of photons spread out in the broad wing portion of the resulting corrected PSF. About 40-60% photons are within $\sim 0.2''$ angular diameter, or 2-3 diffraction-limited core size. Therefore, the optimal design of the AO spectrographs is to match the entrance slit width to the 2-3 diffraction-limited core size to provide high throughput. A smaller width slit could be applied to obtain high spectral resolution, but the throughput dramatically decreases as the slit narrows down. On the other hand, slightly larger than $0.2''$ slit size cannot improve much more throughput due to the wide distribution of the uncorrected photons. Moreover, larger slit size will bring in more sky and thermal background into the spectrograph system and decrease the detectability and spectral resolution.

Because of the low and high order anisoplanatism, the AO corrected field-of-view is limited to about 1 arc min, and image quality degrades dramatically at the edge of the field. However, the relatively small AO corrected FOVs could be still very useful for the multiple object IR AO spectroscopy because the largest size of the present available IR detector such as the 1kx1k InSb array naturally matches the AO corrected FOVs (Fowler et al. 1996).

Though sky coverage by bright natural guide stars with $V \leq 14$ mag. is very small, the image quality corrected by the NGS is much better than that by the LGS. For this special case, about 40% photons are within $0.1''$ diameter. So much narrower slits could be used to maintain the high throughput, but increase the spectral resolution of about a factor of two.

Together, the design of the IR AO spectrographs should at least coordinate the needs of the $0.1''$, $0.2''$ entrance aperture sizes for the LGS and NGS, respectively. Further, in about 10% best seeing conditions, the AO corrected images will be very close to the ideal diffraction limited, much narrower slit width matching the diffraction limited

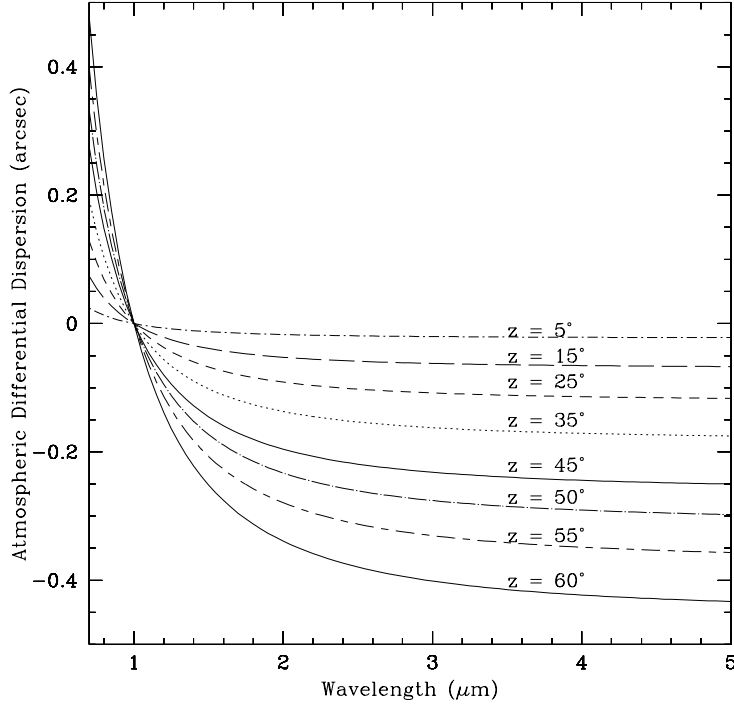


Figure 6. Atmospheric differential dispersion vs wavelength at different zenith angle above Mt. Hopkins ($P = 600$ mmHg, $T = 280$ K, water vapor $P = 8$ mm Hg).

core size, e.g. $0.06''$ in the H band for the MMT 6.5 m, could be used. Including this option in the spectrograph design could significantly increase the spectral resolution.

As we mentioned before, another big potential advantage with the IR AO spectroscopy is that much smaller spectrograph entrance aperture size can help block most sky background which is always associated with the seeing-limited IR spectroscopy. A factor of 5-10 times fainter limit can be reached with the AO spectroscopy if sky background is the dominant one. However, there is always dark current associated with the IR detector, the lowest is about $\sim 0.1 \text{ e s}^{-1}$ (Fowler et al. 1996). If the sky background gets too much dispersed by the spectrograph gratings, then the detector noise, especially dark current, will be the dominant background noise. The extra advantage of smaller slit width to the IR spectroscopy will eventually disappear. Detailed studies of IR background including sky OH emission lines and airglow emission and thermal emission show that $R \sim 2,000$ AO spectroscopy can take full advantage of the narrower slit width (Ge et al. 1997 in preparation).

Another potential concern for the IR AO spectroscopy is the atmospheric differential dispersion, which has been neglected in the seeing limited IR spectroscopy. Figure 6 shows the atmospheric differential dispersion for different zenith angles at different wavelengths above Mt. Hopkins. The dispersed images from the J and K bands could be separated as large as $\sim 0.2''$ if the observations are made at high airmasses. Therefore, the slit loss caused by this dispersion effect could be serious if the spectroscopy covered a large wavelength region. An atmospheric dispersion corrector is needed to correct this effect, or instrument rotator is required to allow all the dispersed images align on the slit.

ACKNOWLEDGEMENTS

We wish to thank Dr. T. Groesbeck, S. Stahl for useful conversations. This work has been supported by the AirForce office of Scientific Research under grant number F 49620-96-1-0366, NSF AST-9421311 and AST-9623788.

REFERENCES

- Beckers, J.M. 1993, *ARA&A*, 31, 13
- Bacon, R. et al. 1995, *A&AS*, 113, 347
- Diego, F. et al. 1995, *MNRAS*, 282, 323
- Ellerbroek, B.L. 1991, Rep. RDA-TR23-1502 (R&D Associate, Albuquerque, N.M., 1991)
- Ellerbroek, B.L. 1994, *JOSA*, 11, 783
- Ellerbroek, B.L., Pompea, S.M., Robertson, D.J., & Mountain, C.M. 1994, *SPIE*, 2201, 421
- Fowler, A.M., et al. 1996, *SPIE proceeding*, 2816, 150
- Fried, D.L. 1994, in *Adaptive Optics for Astronomy* (Kluwer Academic Publishers), eds: Alloin, D.M., & Mariotti J.-M. 25
- Ge, J. et al. 1996, in *Adaptive Optics*, Vol. 13, OSA Technical Digest Series (OSA, Washington DC), 122
- Ge, J. et al. 1997, in *ESO Workshop on Laser Technology for Laser Guide Star Adaptive Optics*, Carching, in press
- Greenwood, D.P. 1979, *JOSA*, 69, 549
- Greenwood, D.P. & Parenti R.R. 1994, in *Adaptive Optics for Astronomy* (Kluwer Academic Publishers), eds: Alloin, D.M., & Mariotti J.-M. 185
- Lambert, D.L. et al. 1990, *ApJL*, 359, L19
- Parenti, R.R. 1992, *Lincoln Laboratory Journal*, 5, 93
- Ridgway, S.T., 1994, in *Adaptive Optics for Astronomy* (Kluwer Academic Publishers), eds: Alloin, D.M., & Mariotti J.-M. 269
- Rigaut, F. 1994, in *Adaptive Optics for Astronomy* (Kluwer Academic Publishers), eds: Alloin, D.M., & Mariotti J.-M. 163
- Sasiela, R.J., *Electromagnetic Wave Propagation in Turbulence: A Mellin Transform Approach*, (Springer-Verlag, 1993).
- Sandler, D.G. et al. 1994, *JOSA*, 11, 925
- Tull, R.G. 1994, *SPIE proceeding*, 2198, 674
- Vogt, S.S., & Schroeder, D.J. 1987, in *Instrumentation for Ground-based Optical Astronomy*, Proc. of Ninth Santa Cruz Summer Workshop in Astronomy and Astrophysics, ed. Robinson, L.B., 3
- Vogt, S.S., et al. 1994, *SPIE proceeding*, 2198, 362